XFEL OSCILLATOR SIMULATION INCLUDING ANGLE-DEPENDENT CRYSTAL REFLECTIVITY *

W.M. Fawley, LBNL, Berkeley, CA 94720, USA†
R.R. Lindberg, K.-J Kim, and Y Shvyd'ko, ANL, Argonne, IL 60439, USA

Abstract

The oscillator package within the GINGER FEL simulation code has now been extended to include angle-dependent reflectivity properties of Bragg crystals. Previously, the package was modified to include frequency-dependent reflectivity in order to model x-ray FEL oscillators[1] from start-up from shot noise through to saturation. We present a summary of the algorithms used for modeling the crystal reflectivity and radiation propagation outside the undulator, discussing various numerical issues relevant to the domain of high Fresnel number and efficient Hankel transforms. We give some sample XFEL-O simulation results obtained with the angle-dependent reflectivity model, with particular attention directed to the longitudinal and transverse coherence of the radiation output.

INTRODUCTION

There has been increasing interest in driving advanced light sources at x-ray wavelengths using electron beams from extremely high repetition rate, high brightness, superconducting accelerators as the electron beam. For MHz and higher repetition rates, FEL's in oscillator configurations become very attractive, presuming appropriate focusing and reflective optics are available at the necessary wavelength. One possibility is based on using Bragg crystals at hard x-ray photon energies [2] for which the net reflectivity per pass can approach 90% or greater. Over the last couple years we have done extensive numerical modeling of XFEL-O configurations using the axisymmetric ($r-z$), polychromatic FEL simulation code GINGER for which an oscillator physics package, including propagation within an optical cavity with mirrors, had been written and used in the mid-1990's (see, *e.g.*, [3]). While the original package had extremely fast execution times as it was contained within the main code itself (unlike the OPC extension to GENESIS [4]), it treated mirrors as having simple angle- and wavelength-independent reflectivity R. As reported previously [5], we added a a λ-dependent mirror reflectivity model in GINGER and used this to examine the predicted output properties for a standard XFEL-O configuration. We have now further extended the oscillator package so that R is now a function simultaenously of both λ and incident angle θ. This new advance is significantly more complicated in terms of the necessary mathematical algorithm and the required structural changes to the code. In the remainder of this paper, we first give some details of the algorithm and other changes to GINGER, then discuss some sample oscillator results at $14.4\,\mathrm{keV}$ photon energy, and conclude with a brief summary.

* This work was supported under the auspices of the Office of Science, U.S. DOE under Contracts No. DE-AC02-06CH11357 (ANL) and No. DE-AC02-05CH11231 (LBNL).

† WMFawley@lbl.gov

IMPLEMENTATION OF THE λ- AND θ-DEPENDENT REFLECTIVITY MODEL

The original GINGER oscillator physics package presumes a constant mirror reflectivity and uses a Huygens integral method (see Eq. 16.94 in [6]) to transport the outgoing FEL radiation from the undulator exit to the various mirror surfaces and back to the undulator entrance. At the beginning of the simulation, the code calculates the complex matrix T_{ij} with

$$E_{entrance}(r_i,t) = \sum_j T_{ij}\, E_{exit}(r'_j,t) \qquad (1)$$

where index i refers to undulator entrance and j to undulator exit. The matrix T includes effects due to mirror curvature, mirror holes, and free space propagation. Imperfect reflectivity (*i.e.,* $|R^2|<1$) is currently presumed spatially to have a constant value over the non-holey mirror surfaces. Note that for the case that R is solely a function $R_0(r)$ of position (and not of angle of incidence), the matrix T and the underlying Huygens integral are defined completely in configuration space so no transforms to either the frequency or transverse wavenumber domain are necessary for evaluation.

Even before considering wavelength and angle-dependent reflectivity, the relatively low pass-to-pass gain and large Fresnel numbers relevant to many XFEL-O configurations posed numerical difficulties due to the oscillatory nature of the Huygens integral kernel

$$r'\, J_0(k_s r r'/L)\, \exp\left[\, ik_s(r^2+r'^2)/2L\,\right] \qquad (2)$$

Here r' is the source point, r the observation point, L the effective longitudinal separation, and $k \equiv 2\pi/\lambda_s$ the wavenumber corresponding to FEL resonance. Following a suggestion in [7], we overcame this problem by reexpressing $J_0(x) \equiv \frac{1}{2}[H_0^{(1)}(x) + H_0^{(2)}(x)]$ for $x \geq 3$ where H_0 is the Hankel function. For large x, this subsitution isolates the fast oscillation term of J_0 and makes accurate numerical integration over r' far more easy. Within the undulator, GINGER uses a radially non-uniform grid for the FEL radiation calculations; the intermediate gridding on the mirror surfaces is also typically non-uniform in order to maximize

computational efficiency and accuracy. For $N_R \sim 128$ radial grid cells within the undulator and ~ 256 cells on the mirror surfaces (the latter number is relevant only to the one-time calculation of T_{ij}), we found that numerical propagation losses could be limited to 0.2% or less per pass. Even if one needs to use 512 or greater zones to grid the mirror surfaces, this only affects the size of the intermediate matrices needed for the one-time calculation of T but not the actual size of T itself.

Normally the GINGER code operates completely in the time-domain, with all spectral decomposition done only after completion of the FEL simulation by a completely separate post-processor code. However, our extension last year to a λ-dependent Bragg crystal reflectivity model required that after each and every oscillator pass a Fourier transform from $E(t)$ to $E(\lambda)$ be done at each radial grid zone, following which the complex $R(r,\lambda) \equiv R_0(r) \times R_c(\lambda)$ is applied once per crystal surface, and then finally the resultant $E(r',\lambda)$ is transformed back to the time domain. Since this is done only once per pass, the computational cost is fairly negligible. The complex $R_c(\lambda)$ is read in as a simple lookup table at the beginning of the simulation with linear interpolation done between table values. Moreover, since $R_c(\lambda)$ was presumed to be $r-$ and angle-independent, the T calculated for the nominal case of $\lambda-$independent $R_0(r)$ can be used unchanged in the $\lambda-$ domain other than multiplication by the $r-$independent $R_c(\lambda)$.

Extension to a full $R_C(\lambda,\theta)$ crystal reflectivity model is significantly more complex because the θ dependence is not independent of λ and *visa-versa*. Referring to Fig. 1, one sees for the XFEL-O configuration currently of most interest to us that the undulator exit-to-entrance propagation path has a central portion involving Bragg crystals, and outer portions involving simple grazing-incidence focusing optics (currently presumed to have λ- and θ-independent reflectivity). Consequently, the transfer matrices for each of the two outer portions can be calculated using the original Huygens integral methods. By contrast, the central region with angle- and λ-dependent crystal reflectivity requires propagation in the frequency and transverse wavenumber $p_\perp = k_s\theta$ domains. Propagation from z' to z is then simply

$$E(\lambda,p_\perp,z) = \exp\left(ip_\perp^2(z-z')/2k_s\right) \times R(\lambda,p_\perp) \times E(\lambda,p_\perp,z') \qquad (3)$$

Since a Hankel transform pair must be done on every pass for each λ of interest, we adopted the pseudo-fast Hankel transform methods (which exploit a special mathematical convolution of $H(s)$ on an exponential grid) described in Refs. [8] and [9] for computational speed. Good numerical accuracy required $\sim$ 512 grid points in $p_\perp$ and r (at the crystal surfaces) over a full range of 10^4 in scale. Since this is typically much greater than the number of radial grid zones ($N_R \leq 128$) within the undulator, for computational efficiency we transform $E(r,t)$ to the frequency domain immediately upon exit from the undulator and do not transform back to the time domain until undulator entrance for the next pass. This thus requires $2N_R$ FFT's of length N_t, the number of photon slices in time. Because only a limited number of frequency points have any significant crystal reflectivity, it is *only* for these points for which we must do the Hankel transform pair; points outside the reflectivity region had $E(\lambda,r)$ set to zero. Altogether, one must do approximately $2\epsilon N_t$ Hankel transforms of length 512 with $\epsilon \approx 1/4$. We implemented a simple bilinear lookup scheme in a simple $R(\lambda,p_\perp)$ table input at the beginning of the simulation run.

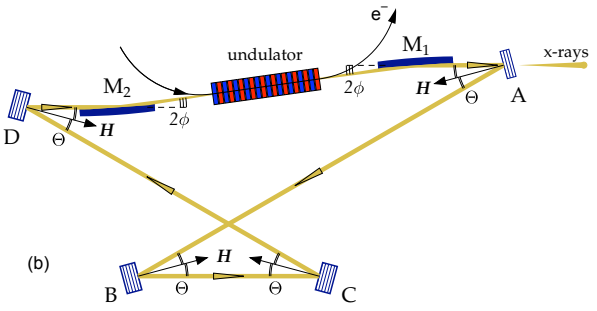

Figure 1: XFEL-O configuration with four Bragg crystal reflections on the return path.

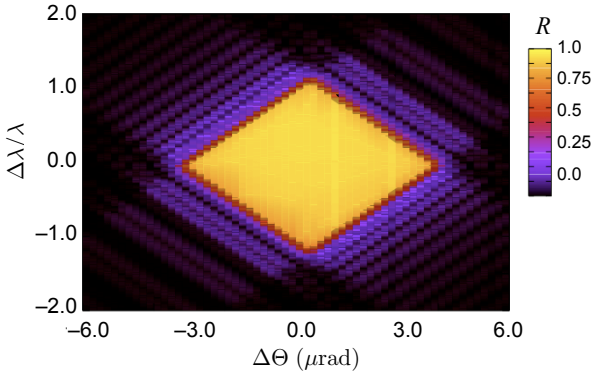

Figure 2: Absolute value of reflectivity plotted as function of angle of incidence and wavelength (in units of 10^{-6}).

Although the necessity of Hankel transforms has requires additional computation relative to a simple $R(\lambda)$ function, the overall computation time is still heavily dominated by the "normal" FEL simulation within the undulator since typically 100 or more z steps are required. In the future we may explore the "FHA" transform triplet as an alternative to doing direct Hankel transforms but it is unclear if this will either increase the speed or accuracy significantly, in particular because of the need to do an Abel transform on a cyclindrical grid.

AN EXAMPLE OF A GINGER 14.4-KEV XFEL-O SIMULATION

We used the new capabilities of the code to model startup from noise of an XFEL oscillator at 14.4 keV photon energy designed around the C337 peak reflectivity proper-

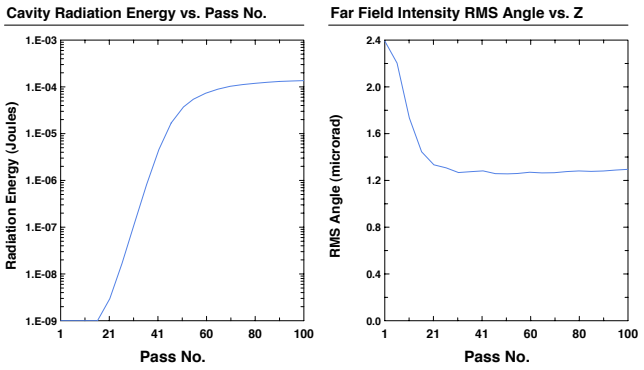

Figure 3: Intracavity pulse energy (left) for a sample 14-keV XFEL-O example and the time-integrated far field angle (right) of the intracavity radiation as a function of pass number.

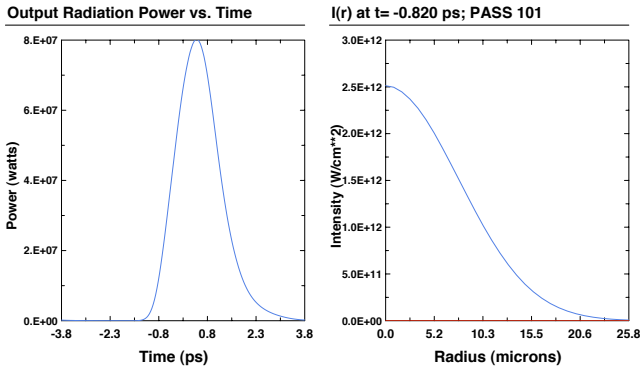

Figure 4: Temporal and radial power profile for pass 101 as measured in the center of the undulator.

ties of diamond Bragg crystals. The electron beam properties were: $I = 20\,\mathrm{A}$, $\sigma_t = 1\,\mathrm{ps}$ in a Gaussian profile, $E = 7\,\mathrm{GeV}$, $\sigma_E = 1.4\,\mathrm{MeV}$, and $\varepsilon_{\perp,N} = 0.2\,\mathrm{mm\text{-}mrad}$. The linearly-polarizded undulator had an RMS K of 0.974 and a period of $16.56\,\mathrm{mm}$. The 1-mm diameter focusing mirrors had $R_c = 52\,\mathrm{m}$ and were separated by 100 m. The simulation grid had $\Delta z = 50\,\mathrm{mm}$ and used a slice separation of $40\,\mathrm{fs}$. For the Hankel transforms, there were 768 points in r and $p_\perp$; this is equivalent to a 1.25% increase from grid point to grid point on the exponential grid. We should mention that we artificially removed the linear term in $\phi(t)$ corresponding to the crystal reflectivity that produces an effective delay in radiation arrival time from pulse to pulse. Physically, one would compensate for this delay by shortening the return path in the cavity. Typical CPU run times for 100 passes were ~ 1 hour on a 2010-era single processor (unlike the amplifier coding, the oscillator package in GINGR currently cannot run in parallel).

Figures 3 through 5 show various diagnostics quantities for the GINGER simulation. The growth of intracavity pulse energy versus pass number are shown in Fig. 3. One sees a growth rate of $\sim 25\%$ per pass with saturation occurring after about 80 passes. Similarly, the RMS far field angle of the radiation (integrated temporally over the pulse) drops down to an value of about 1.3 microradians after 25 passes, well within the envelope corresponding to the reflectivity acceptance shown in Fig. 2. The temporal profile (Fig. 4a) out the intracavity power at pass 100 is quite smooth with noticeable asymmetry from head to tail. Time-resolved diagnostics of the radial intensity (Fig. 4b) and phase profiles show excellent beam quality with M^2 of 1.1 or less and 99.9% of the power in the lowest order TEM00 mode. This too would be expected from the limited angular reflectivity of the Bragg crystals. Figure 5 shows snapshots of the power spectra at various passes on a semi-log scale. By pass 36 the spectrum is quite clean and has a normalized bandwidth of below 10^{-7}. So, within the obvious caveat that these simulations have not included degradation effects such as mirror distortions and surface roughness, unwanted tilts, and undulator field errors, the results suggest that extremely high quality FEL output is possible in theory presuming the electron beam has the necessary 6D brightness to support XFEL-O lasing.

SUMMARY

In this paper we have discussed some of the changes made to GINGER to allow modeling of XFEL oscillator configurations employing Bragg crystal reflectors. In particular we have extended the cavity propagation algorithm to include wavelength- and angle-dependent reflectivity. This change required the introduction of Hankel transforms and improved evaluation of the Huygens Integral due to the high Fresnel number associated with the XFEL-O design. Application to a standard test case shows quite high quality output, both in terms of longitudinal and transverse coherence.

REFERENCES

[1] R.R. Lindberg *et al.*, submitted to *PRST-AB*, 2010.

[2] R. Colella and A. Luccio. *Optics Comm.*, **50**, 41, (1984).

[3] S.J. Hahn *et al.*, *Nucl. Inst. Meth.*, **A358**, 167 (1995).

[4] J.G. Karssenberg *et al.*, Paper TUPPH037 "FEL-Oscillator Simulations with Genesis 1.3", in Proc. FEL06 (Berlin), (2006).

[5] R.R. Lindberg *et al.*, Paper WEPC40 "Simulation Studies of the X-ray Free-Electron Laser Oscillator", Proc. FEL09 (Edinburgh) (2009).

[6] A. E. Siegman, *LASERS*, Univ. Science Books (Mill Valley, CA, USA, 1986).

[7] W.H. Southwell, *Opt. Letters*, **3**, 100 (1978).

[8] Q-H Liu and W.C. Chew, *Radio Sci.*, **2**, 1009 (1994).

[9] Q-H Liu and Z.Q. Zhang, *Appl. Optics*, **38**, 6705 (1999).

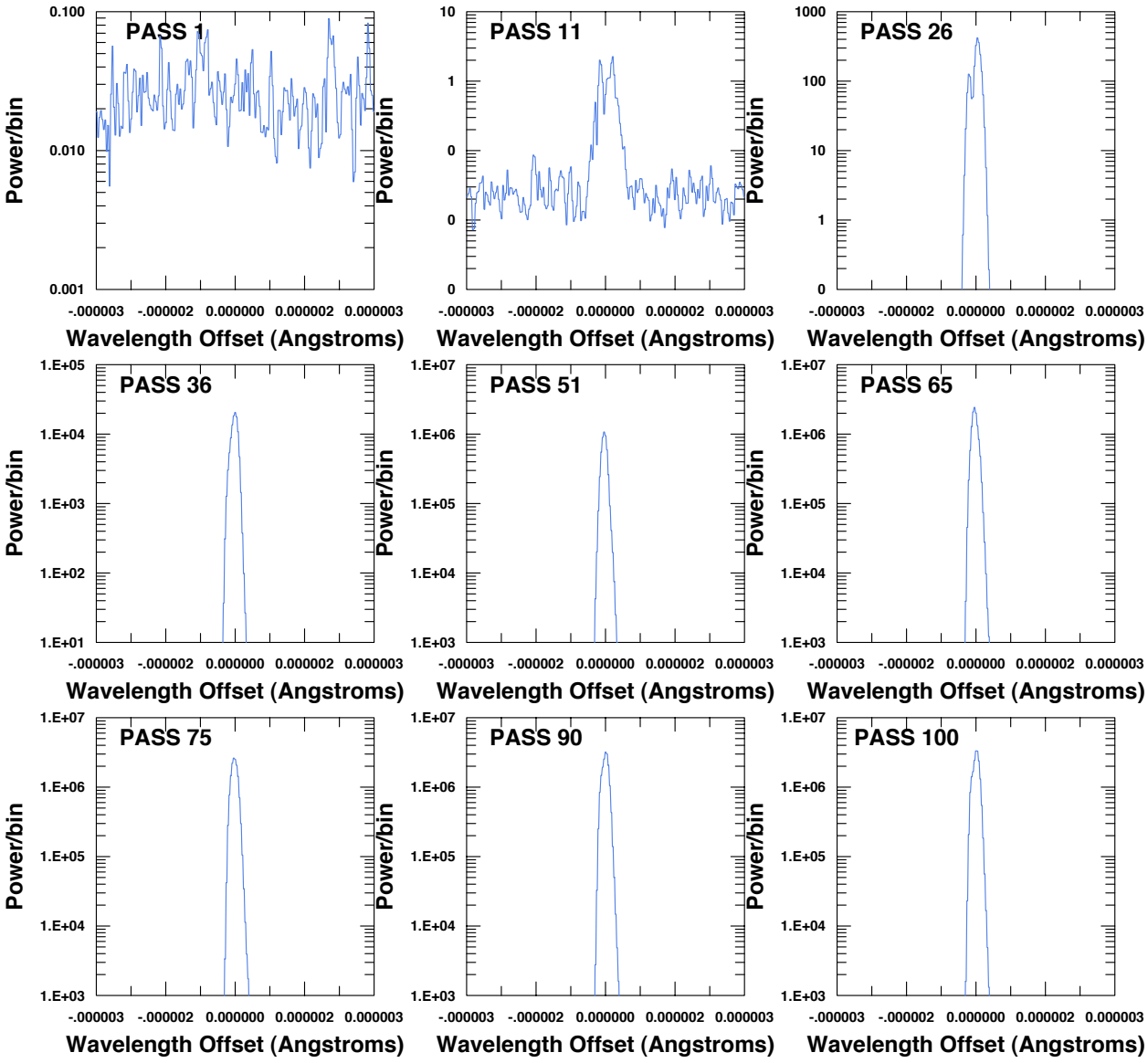

Figure 5: Snapshots of spectra at various pass numbers; note the semilog scale. The central wavelength in the simulation was 0.86Å (14.4 keV).